Micron-scale holes terminate the phage infection cycle

Jill S. Dewey[a,1], Christos G. Savva[b,1], Rebecca L. White[c,2], Stanislav Vitha[b], Andreas Holzenburg[a,b,c], and Ry Young[a,3]

Departments of [a]Biochemistry and Biophysics and [c]Biology, and [b]Microscopy and Imaging Center, Texas A&M University, College Station, TX 77843

Holins are small phage-encoded proteins that accumulate harmlessly in the cytoplasmic membrane during the infection cycle until suddenly, at an allele-specific time, triggering to form lethal lesions, or "holes." In the phages λ and T4, the holes have been shown to be large enough to allow release of prefolded active endolysin from the cytoplasm, which results in destruction of the cell wall, followed by lysis within seconds. Here, the holes caused by S105, the λ-holin, have been captured in vivo by cryo-EM. Surprisingly, the scale of the holes is at least an order of magnitude greater than any previously described membrane channel, with an average diameter of 340 nm and some exceeding 1 μm. Most cells exhibit only one hole, randomly positioned in the membrane, irrespective of its size. Moreover, on coexpression of holin and endolysin, the degradation of the cell wall leads to spherically shaped cells and a collapsed inner membrane sac. To obtain a 3D view of the hole by cryo-electron tomography, we needed to reduce the average size of the cells significantly. By taking advantage of the coupling of bacterial cell size and growth rate, we achieved an 80% reduction in cell mass by shifting to succinate minimal medium for inductions of the *S105* gene. Cryotomographic analysis of the holes revealed that they were irregular in shape and showed no evidence of membrane invagination. The unexpected scale of these holes has implications for models of holin function.

bacteriophage | cryoelectron tomography | *Escherichia coli* | holin | lambda

Bacteriophage lysis, the most frequent cytolethal event in the biosphere, is a precisely scheduled process controlled by proteins of the holin family (1). Holins are an extremely diverse class of small phage-encoded membrane proteins (2). The best studied holin is S105, a 105-residue polypeptide with three transmembrane domains (TMDs) encoded by the *S* gene of phage λ (3). Throughout the period of late gene expression and particle assembly, S105 accumulates in the cytoplasmic membrane of *Escherichia coli* without any effect on its integrity (4). Suddenly, at a programmed time, S105 triggers to form a lesion, or hole, in the membrane; this allows the λ-endolysin, R, to escape from the cytoplasm and attack the cell wall (2). In phages of Gram-negative hosts, there is a third step to complete the lysis pathway involving a protein or protein complex, the spanin, which connects the cytoplasmic and outer membranes (5, 6). In λ, the spanin complex consists of the cytoplasmic membrane protein, Rz, and the outer membrane lipoprotein, Rz1. This complex is essential for lysis in media containing millimolar concentrations of divalent cations, and thus is thought to act by disrupting the outer membrane, possibly by fusion with the inner membrane (6).

Although the S105 holin has been extensively studied using genetic and biochemical approaches (3, 4, 7–9), nothing is known about the membrane holes except that they are nonspecific and large enough to allow escape of fully folded tetrameric R-β-galactosidase chimeras (>450 kDa), indicating that they are of unprecedented size for channels made by integral membrane proteins (10). Recently, cryo-electron microscopy (cryo-EM) studies of detergent-purified S105 revealed large ring assemblies with two main size groups consisting of 18 and 20 protomers, respectively, with the majority class, 18mers, having an inner diameter of ~8.5 nm (9). S105 in these purified complexes retained

α-helical content and protease sensitivity consistent with the membrane topology in vivo, as determined by genetic and biochemical experiments (3). However, the nature of the S105 lesion in the host membrane has remained elusive. The luminal diameters observed are not consistent with the ability to release endolysin-β-galactosidase chimeras with a mass of ~0.5 MDa. Attempts to visualize the membrane lesions by conventional ultrathin-section EM have been unsuccessful (11), in part because of the structural deformations associated with the multiple fixation, dehydration, and staining steps (12).

Rapid freezing at liquid ethane temperatures allows complete preservation of biological material smaller than ~2 μm in size in a native hydrated environment (13, 14). Furthermore, the millisecond fixation allows time-dependent biological processes to be captured essentially instantaneously (15). We reasoned that by examining cells expressing *S105* in the absence of *R*, *Rz*, and *Rz1*, we could observe the sole effect of the holin on the host cell. Furthermore, by using cryo-EM, we would be able to image the cells in a physiologically relevant state. The results of these studies are discussed in terms of a model for the molecular pathway of holin-mediated lysis.

Results

Expression of *S105* Leads to Large Membrane Gaps in the *E. coli* Inner Membrane. To examine the effect of S105 on the host, we used *E. coli* strains expressing the holin in the presence and absence of the endolysin R and the spanin complex proteins Rz and Rz1 (Fig. 1*A*). It was important to characterize the lysis behavior of the strains before their imaging by cryo-EM. Cultures expressing *S105* with and without *R* were grown and induced for expression of the lysis genes (Fig. 1*B*). The strain harboring pSRRzRz1, with functional alleles of all the genes of the λ-lysis cassette, lysed as expected at ~50 min. The strain carrying pS, expressing *S105* alone, ceased growth at 50 min, indicative of hole formation in the cytoplasmic membrane; however, because of the absence of endolysin activity, it did not undergo lysis. To visualize the effect of S105 alone on the host membrane, a 60-min sample of an induced pS culture was plunge-frozen into liquid ethane without any further manipulation (i.e., concentrating, washing). Specimens were then imaged under liquid nitrogen temperatures and low-dose conditions, revealing rod-shaped cells with intact outer membranes. On closer examination, about half of the cells displayed an apparent discontinuity in the inner membrane density (Figs. 2*A* and 3*A*). These gaps ranged in size from 88 nm to 1.2 μm, with an average size of ~340 nm (Figs. 2 *B–D* and 3*B*). The lesions were not localized to a
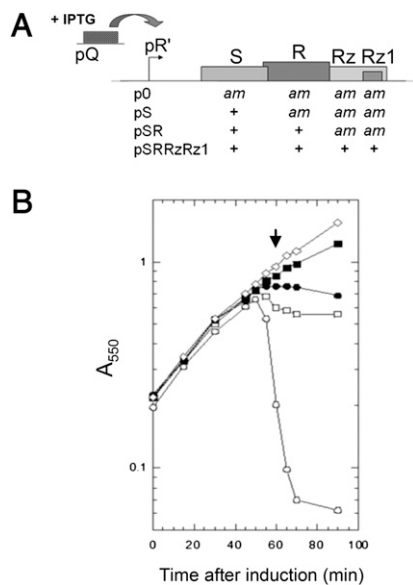
Fig. 1. Induction of lambda lysis genes. (*A*) Plasmids used in this study. (*B*) Lysis curves of cultures carrying the following: no S105 plasmid (◇), p0 (■), pS(•), pSR supplemented with 10 mM MgCl₂ (□), or pSRRzRz1 (○).The arrow shows the 60-min time point at which samples were taken for cryo-EM. IPTG, isopropyl-β-ᴅ-thiogalactopyranoside.

specific region in the inner membrane but appeared randomly throughout its periphery, irrespective of size (Fig. 3 *C* and *D*). Taking into account the geometry of viewing in the vitreous ice, the observed diameters, and the random positioning of the lesions, calculations indicated that there must be approximately two holes per cell (Fig. S1). To confirm that these inner membrane gaps were associated with S105 function, cells expressing an isogenic null *Sam* plasmid (p0) were also visualized. Among 45 cells from two different experiments, none displayed inner membrane discontinuity (Fig. 3*A* and Fig. S2*B*). These data indicate that the large gaps observed in the cells expressing *S105* are, in fact, the lethal holes that allow the endolysin access to the cell wall immediately before cell lysis. The unprecedented size of the holes, more than 10-fold larger than those formed by pore-forming cytolysins (16), accounts for the ability of S105 to cause release of unrelated prefolded endolysins with heterologous structure (2) and of the megadalton-scale R-β-galactosidase chimeras (10).

Cryo-tomography of the S105 Lesions. To visualize the overall structure of the S105 lesion, cryo-electron tomography was carried out on *E. coli* cells expressing *S105*. Initial attempts were complicated by the large size of the LB-grown cells; the electron path through the specimen at 60° is twice that at a tilt of 0°. Hence, a cell with a width of ~1 μm results in images of very poor signal because of the multiple inelastic scattering events despite the use of an energy filter. In an attempt to reduce the size of the cells, we took advantage of the coupling between cell mass and growth rate (17) and tested several minimal medium conditions (18) for the ability to support the slowest possible growth rate but still allow the precisely scheduled lysis characteristic of cells grown in rich medium. Among several carbon sources tested, succinate was found to support a doubling time of 80 min and preserved rod-shaped morphology; induction of the fully functional lysis cassette led to sharply defined lysis at 30 min after induction (Fig. S3). Phase-contrast microscopy as well as cryo-EM examination revealed that the average cell length and diameter were reduced by >30%, leading to a final relative volume ~20% of that observed in LB (Fig. S4). We examined
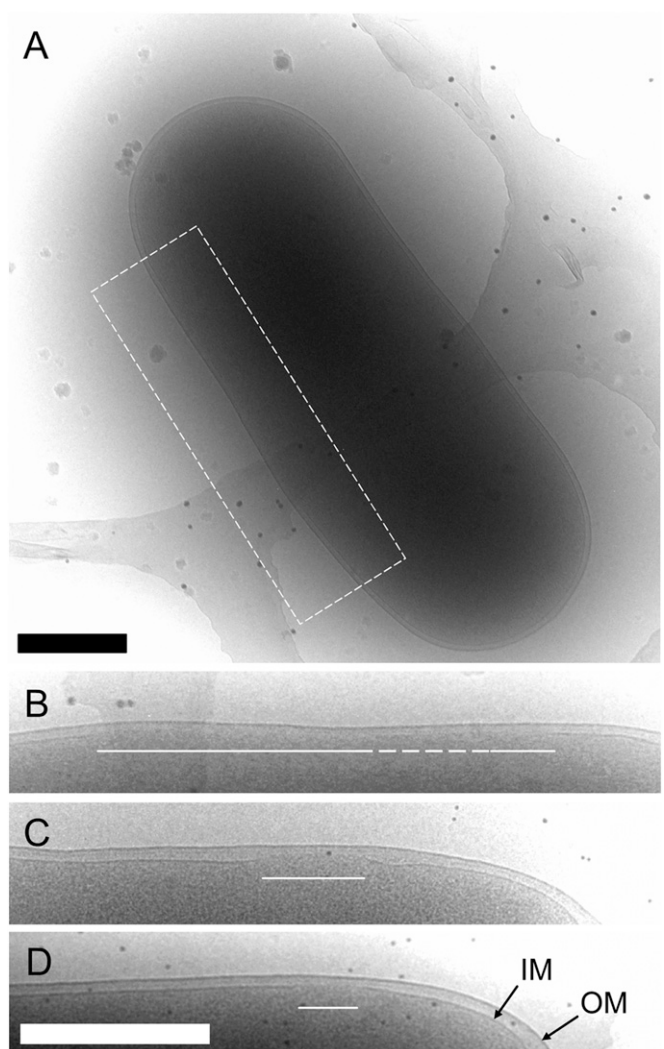

Fig. 2. Cryo-EM of the S105 lesion. Cells were grown and imaged as described. (*A*) Cell expressing *S105* is shown. (*B*) Area enclosed in the white dashed box is shown enlarged. The white solid lines indicate the location and extent of the lesion. The dashed white line indicates an area of semicontinuous membrane density. (*C* and *D*) Close-up views of the S105 lesions from two other cells. (Scale bar: 500 nm.) IM, inner membrane; OM, outer membrane.

induced cells for lesions smaller than ~200 nm to acquire tomographic data completely spanning a hole. Two 3D reconstructions of cells induced in succinate minimal medium were obtained (Fig. 4 and Fig. S5). Slices through the tomogram (Fig. 4) show the appearance of a lesion with a maximum diameter of ~130 nm across the x–y plane and its subsequent disappearance over a z range of ~125 nm. The actual height of the lesion is less when taking into account cell elongation effects along z attributable to the missing wedge (19, 20). Segmentation of the cell envelope densities in both tomograms (Fig. 4*B* and Fig. S5*C*) revealed that the lesion in each case was irregular in shape. Although irregular, the lesions resemble a roughly circular shape (i.e., they are not elongated along a particular axis.)

The Holin–Endolysin System Effects Dramatic Changes on *E. coli* Immediately Before Lysis. Having observed the effect of S105 alone on the cell envelope, we sought to visualize cells under conditions that permit complete host cell lysis (i.e., with coexpression of the endolysin R) (Fig. 1). In images of samples taken at 60 min, the great majority of these cells had undergone com-
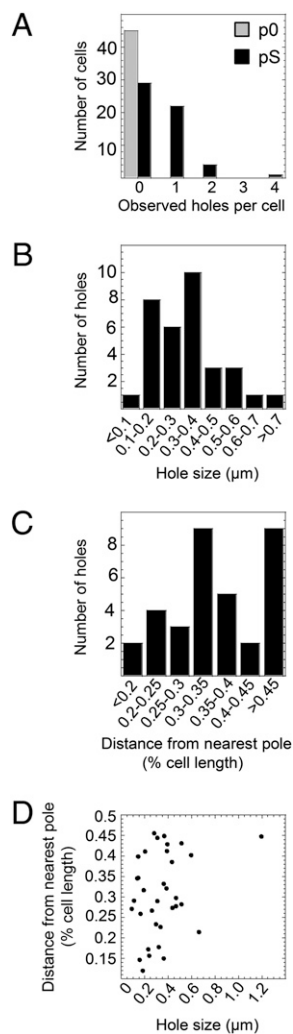
Fig. 3. Quantification of the number of S105 holes per cell (*A*), hole size variation (*B*), hole localization (*C*), and relation of hole size to location (*D*).

plete lysis, as evident from the presence of cellular debris. However, we were able to capture rare instances of cells that had not yet lysed. These cells had lost the characteristic rod shape of *E. coli* and were completely spherical (Fig. S6). Because neither *Rz* nor *Rz1* is functional, the outer membranes of these cells were still intact. Nevertheless, the inner membrane sacs were collapsed, with evident release of cytoplasmic contents. As shown in Fig. 1*B*, in the absence of *Rz* or *Rz1* function, lysing cells can be stabilized in this spherical morphology if millimolar concentrations of divalent cations are supplied in the medium (21, 22). Samples taken from an induced pSR culture in medium supplemented with 10 mM MgCl₂ were imaged and found to contain a significantly larger number of intact yet spherical cells similar to the rare unlysed cells in the absence of metal ions. This allowed us to capture various levels of inner membrane disruption, ranging from large membrane gaps to a total collapse of the inner membrane sac (Fig. S7). In addition, as a result of the destruction of the murein, most cells exhibited a significant separation of the inner and outer membranes. No instances of punctate zones of adhesion, or Bayer's patches (23, 24), between the membranes were observed, supporting the notion that they either require the presence of the murein or may be artifacts of sample preparation (12, 25). Stages of early cytoplasmic leakage through the S105 hole were also observed. An example is shown in Fig. S8, where a cloud of density proximal to the inner membrane suggested cytoplasmic leakage through a hole. Tilting of the microscope stage confirmed that the leakage originated from a lesion of ∼100 nm in diameter (Fig. S8 *B–D*).

Discussion

The lethal holes caused by the holin–endolysin lysis system of bacteriophages have now been directly observed in cells. Unexpectedly, the size of the membrane holes caused by the S105 protein in terminating the λ-infection cycle exceeds by more than an order of magnitude that reported for any other membrane lesion in biology, the largest of which are the ∼30-nm pores formed by the cholesterol-dependent cytolysins (16, 26). Tomographic analysis confirmed that membrane gaps observed in projection represented actual holes rather than invaginations or deformations. In addition, it could be established that the holes were irregular in shape, unlike the highly symmetrical cytolysin pores that make up the next largest membrane holes observed to date (26). These results contradict the previous ultrastructural study, which failed to detect any interruptions in the integrity of the cytoplasmic membrane after function of the S holin (11); however, the previous work used thin sections of cells subjected to harsh fixation and dehydration steps.

The existence of holes of such unprecedented size is even more remarkable, considering that throughout the infection cycle until the moment of triggering a few seconds before lysis, the accumulation of S105 in the host membrane has no effect on the integrity of the membrane or its energy-generating capacity (4). This reflects the extreme but opposed selection pressures on holin function as the timer for the latent period (i.e., the holin should not compromise the capacity of the host for macromolecular synthesis until the programmed instant of triggering). However, after triggering, it should effect a rapid efficient release of the cytoplasmic endolysin, and thus minimize the delay between triggering, which terminates macromolecular synthesis, and the liberation of the progeny virions. It is even more remarkable that the timing of this all-or-nothing event can be adjusted drastically with a single missense change throughout the sequence of the λ-holin (8, 27) and, indeed, of other unrelated holins (28, 29), of which there is staggering diversity of sequence and topology (2).

Although the molecular basis of holin triggering is still unknown, the results presented here provide a clear basis for the oldest observation about holin physiology, that bacterial respiration and macromolecular synthesis cease when S triggers (11, 30, 31). A single hole of this size would be incompatible with the maintenance of either process. Importantly, although the formation of these holes and its temporal scheduling are unambiguously and solely dependent on holin function (2), the role of the S105 protein in the structure of the large lesions is not established. The 8–9-nm ring structures formed by purified S105 in detergent (9) are orders of magnitude too small to represent the membrane lesions described here. Although we as yet have no direct evidence addressing whether S105 participates directly in the holes, alternatives are more difficult conceptually. One extreme alternative is that the triggering of S105 causes a small channel to form, perhaps on the scale of the detergent rings, resulting in collapse of the membrane energization, local disruption in the organization of the lipid, and then propagation of that distortion attributable to loss of tensile strength of the bilayer, perhaps forcing the imposition of hexagonal phase at the edges of the hole. In support of this notion, TMDs have been shown to stabilize nonbilayer lipid structures (32); however, such transitions require a relatively high protein-to-lipid ratio, whereas holins trigger at low protein concentrations (on the order of 10³ per cell for S105) (2). Alternatively, the triggering of S105 could suddenly template the oligomerization and conformational change of unidentified host proteins. This notion is problematic in view of the fact that S105 is also lethal when induced in yeast (33) and mammalian cells (34).
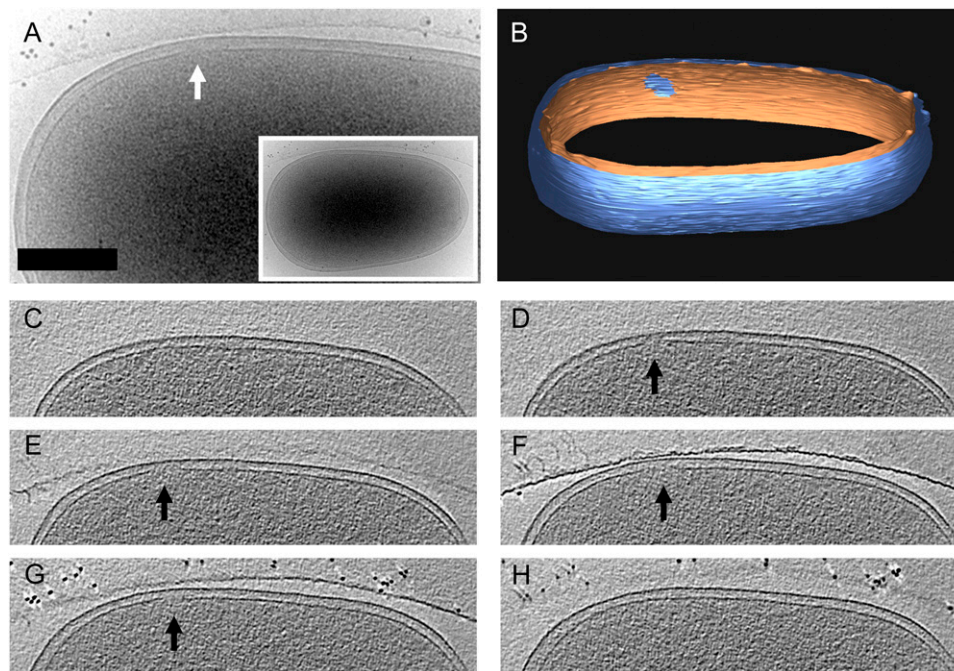
Fig. 4. Cryoelectron tomography of an S105 lesion. (*A*, *Inset*) Cell shown expressing *S105* was tilted ±55°, and a 3D reconstruction was calculated. A close-up of the lesion in projection is highlighted by the white arrow. (*B*) Segmentation of the envelope densities shows the outer membrane (blue) and inner membrane (orange). The 2.6-nm thick slices along z (*C–H*, spaced by 26 nm) show the appearance of a lesion and its subsequent disappearance over a z height of ∼125 nm. Arrows indicate the S105 lesion. (Scale bar: 250 nm.)

In addition, even at these enormous sizes, the perimeters of the holes are consistent with the numbers of S105 holins present at the time of lysis. Because each holin has three TMDs, which, as α-helices, are ∼1 nm in diameter, current estimates of ∼1,000 S105 molecules (35, 36) could correspond to ∼3 μm of perimeter if all the proteins are in the perimeter and each TMD participates. To settle this issue, the ideal approach would be to tag S105 with a fluorescent moiety and use correlative microscopy to demonstrate the presence of the holin in the lesion. However, to date, this technology has not been successfully applied to *E. coli.*

Assuming the simplest idea, that, like all other cytolytic membrane proteins, S105 actually forms the walls of the hole, it is conceivable that smaller S105 rings do form first in the membrane and then coalesce into the macroscopic lesions observed here. Suggestive evidence for this can be seen in the perforated appearance of certain lesions (Fig. 2*B*). Genetic, physiological, and biochemical data have led to a model in which the S105 holin forms large 2D aggregates, or "death rafts," during the lysis pathway (10). The large holes described here can be viewed as supporting the notion that at the time of lethal triggering, the S105 holin exists in such large aggregates, leading to one or a small number of holes rather than many smaller holes distributed throughout the membrane. Current work is aimed at generalizing the observation to other unrelated holins and developing in vitro hole formation methodology using purified S105 holin and liposomes. It is hoped that these approaches will provide further insight into the mysterious mechanism by which the holin manages the temporally scheduled transition between the perfectly maintained membrane integrity of the prehole state and the massive membrane holes described here.

Materials and Methods

Plasmids and Strains. The plasmid pSRRzRz1 is identical to pS105 (37) and carries the λ-lysis gene cassette, *S105RRzRz1*, under the control of the native λ-late promoter, pR′; *S105* is an *S* allele that produces S105, the holin, but not S107, the antiholin, by virtue of the conversion of codon 1 from ATG to CTG. The plasmid pSR is isogenic to pSRRzRz1 but carries the nonsense alleles *RzQ100amRz1W38am*. The plasmid pS is isogenic to pSR except that it carries a

silent mutation (C to T at λ-nt 44,594, which ablates an AatII site) and two nonsense mutations, Q26am and W73am (previously identified as *Rsus54-sus60*) (38), in *R*. The plasmid p0 is isogenic to pS except that the *S105* allele is replaced by the nonsense allele *Sam7* (39). The plasmid pQ is a single-copy vector with λ-gene *Q* cloned under the control of P*ara-lac* (4); pQc is isogenic to pQ except that the *kan*^{R} marker was replaced by *cam*^{R} for use in *kan*^{R} hosts. The hosts used were derivatives of the sequenced *E. coli* K-12 strain, MG1655 (40). A Δ*lacY* derivative was constructed by replacing the *lacY* gene in MG1655 Δ*fhuA lacI*^{q} with Δ*lacY::kan*, in which a *kan* cassette flanked by Flp recombinase sites is substituted for the entire *lacY* reading frame (41). MG1655 Δ*fhuA lacI*^{q} Δ*lacY::kan* was transformed with pQc, creating RY16505. RY16504 is isogenic to RY16505 except that it carries pQ instead of pQc, and the *kan* cassette was excised from Δ*lacY::kan* by Flp recombinase (41).

Growth Conditions and Monitoring. For all experiments except those shown in Fig. S6–S8, the bacterial host used was RY16504. For Fig. S6–S8, the host was RY16505. Cultures were supplemented with 100 μg/mL ampicillin and either 40 μg/mL kanamycin (RY16504) or 10 μg/mL chloramphenicol (RY16505). In addition, pSR cultures were supplemented with 10 mM MgCl$_2$, which stabilizes the outer membrane in the absence of *RzRz1* function. For cultures grown in LB, 100 μL of overnight cultures grown in LB supplemented with the appropriate antibiotics, harboring the indicated plasmids, was used to inoculate 25 mL of LB. The identical procedure was used for succinate minimal media except that 10 μL of overnight cultures was used for inoculation. All cultures were induced with 1 mM isopropyl-β-D-thiogalactopyranoside at A_{550} = 0.2 (for lysis curves) or A_{550} = 0.4 (for cryo-EM).

Cryo-EM and Cryotomography. For cryo-EM, cells were withdrawn 60 min after induction, mixed with BSA-coated gold tracer (10 or 25 nm), and immediately applied to C-FLAT (CF-4/2-2C) or homemade lacey carbon-coated grids that had been glow-discharged just before use. Grids were then plunge-frozen in ethane using an FEI Vitrobot. Specimens were loaded on a GATAN 626 cryoholder and observed with an FEI Tecnai G^2 F20 transmission electron microscope equipped with a GATAN Tridiem imaging filter using zero-loss imaging and low-dose conditions with typical doses of 3–5 e$^-$/Å^2 per image. For cryo-electron tomography, specimens were prepared as above but cells were gently concentrated 20-fold by vacuum filtration through a 0.22-μm filter. Tilt series were acquired automatically using FEI Xplore3D software and the Saxton tilt scheme (42). The tilt range varied from ±53° to ±60°, and the total electron dose for each series was kept below 100 e$^-$/Å^2. Tilt-series alignments, 3D

reconstructions, and tomogram segmentations were carried out using the IMOD (43) tomography package. Tomograms were filtered using nonlinear anisotropic diffusion (44) as implemented in the IMOD package.

1. Young R, Wang IN (2006) Phage lysis. *The Bacteriophages*, ed Calendar R (Oxford Univ Press, New York), 2nd Ed, pp 104–128.
2. Wang IN, Smith DL, Young R (2000) Holins: The protein clocks of bacteriophage infections. *Annu Rev Microbiol* 54:799–825.
3. Gründling A, Bläsi U, Young R (2000) Biochemical and genetic evidence for three transmembrane domains in the class I holin, lambda S. *J Biol Chem* 275:769–776.
4. Gründling A, Manson MD, Young R (2001) Holins kill without warning. *Proc Natl Acad Sci USA* 98:9348–9352.
5. Summer EJ, et al. (2007) *Rz/Rz1* lysis gene equivalents in phages of Gram-negative hosts. *J Mol Biol* 373:1098–1112.
6. Berry J, Summer EJ, Struck DK, Young R (2008) The final step in the phage infection cycle: The Rz and Rz1 lysis proteins link the inner and outer membranes. *Mol Microbiol* 70:341–351.
7. Bläsi U, Chang CY, Zagotta MT, Nam KB, Young R (1990) The lethal lambda S gene encodes its own inhibitor. *EMBO J* 9:981–989.
8. Gründling A, Bläsi U, Young R (2000) Genetic and biochemical analysis of dimer and oligomer interactions of the lambda S holin. *J Bacteriol* 182:6082–6090.
9. Savva CG, et al. (2008) The holin of bacteriophage lambda forms rings with large diameter. *Mol Microbiol* 69:784–793.
10. Wang IN, Deaton J, Young R (2003) Sizing the holin lesion with an endolysin-beta-galactosidase fusion. *J Bacteriol* 185:779–787.
11. Reader RW, Siminovitch L (1971) Lysis defective mutants of bacteriophage lambda: On the role of the S function in lysis. *Virology* 43:623–637.
12. Kellenberger E, et al. (1992) Artefacts and morphological changes during chemical fixation. *J Microsc (Paris)* 168:181–201.
13. McIntosh R, Nicastro D, Mastronarde D (2005) New views of cells in 3D: An introduction to electron tomography. *Trends Cell Biol* 15:43–51.
14. Dubochet J, et al. (1988) Cryo-electron microscopy of vitrified specimens. *Q Rev Biophys* 21:129–228.
15. Berriman J, Unwin N (1994) Analysis of transient structures by cryo-microscopy combined with rapid mixing of spray droplets. *Ultramicroscopy* 56:241–252.
16. Tweten RK (2005) Cholesterol-dependent cytolysins, a family of versatile pore-forming toxins. *Infect Immun* 73:6199–6209.
17. Bremer H, Dennis PP (1996) Modulation of chemical composition and other parameters of the cell by growth rate. *Escherichia coli and Salmonella: Cellular and Molecular Biology*, ed Neidhart FC (ASM, Washington, DC), 2nd Ed.
18. Pierucci O (1978) Dimensions of *Escherichia coli* at various growth rates: Model for envelope growth. *J Bacteriol* 135:559–574.
19. Radermacher M (1992) Weighted back-projection methods. *Electron Tomography*, ed Frank J (Plenum, New York).
20. Ford RC, Holzenburg A (2008) Electron crystallography of biomolecules: Mysterious membranes and missing cones. *Trends Biochem Sci* 33:38–43.
21. Casjens S, Eppler K, Parr R, Poteete AR (1989) Nucleotide sequence of the bacteriophage P22 gene *19* to *3* region: Identification of a new gene required for lysis. *Virology* 171:588–598.
22. Young R, Way J, Way S, Yin J, Syvanen M (1979) Transposition mutagenesis of bacteriophage lambda: A new gene affecting cell lysis. *J Mol Biol* 132:307–322.
23. Bayer ME (1968) Areas of adhesion between wall and membrane of *Escherichia coli*. *J Gen Microbiol* 53:395–404.
24. Bayer ME (1974) Ultrastructure and organization of the bacterial envelope. *Ann NY Acad Sci* 235:6–28.
25. Hobot JA, Carlemalm E, Villiger W, Kellenberger E (1984) Periplasmic gel: New concept resulting from the reinvestigation of bacterial cell envelope ultrastructure by new methods. *J Bacteriol* 160:143–152.
26. Tilley SJ, Orlova EV, Gilbert RJ, Andrew PW, Saibil HR (2005) Structural basis of pore formation by the bacterial toxin pneumolysin. *Cell* 121:247–256.
27. Raab R, Neal G, Sohaskey C, Smith J, Young R (1988) Dominance in lambda S mutations and evidence for translational control. *J Mol Biol* 199:95–105.
28. Ramanculov E, Young R (2001) Genetic analysis of the T4 holin: Timing and topology. *Gene* 265:25–36.
29. Rydman PS, Bamford DH (2003) Identification and mutational analysis of bacteriophage PRD1 holin protein P35. *J Bacteriol* 185:3795–3803.
30. Adhya S, Sen A, Mitra S (1971) *The Role of Gene S* (Cold Spring Harbor Lab Press, Cold Spring Harbor, NY).
31. Josslin R (1971) The effect of phage T4 infection on phospholipid hydrolysis in *Escherichia coli*. *Virology* 44:94–100.
32. Siegel DP, et al. (2006) Transmembrane peptides stabilize inverted cubic phases in a biphasic length-dependent manner: Implications for protein-induced membrane fusion. *Biophys J* 90:200–211.
33. Garrett J, Bruno C, Young R (1990) Lysis protein S of phage lambda functions in *Saccharomyces cerevisiae*. *J Bacteriol* 172:7275–7277.
34. Agu CA, et al. (2007) Bacteriophage-encoded toxins: The lambda-holin protein causes caspase-independent non-apoptotic cell death of eukaryotic cells. *Cell Microbiol* 9:1753–1765.
35. Zagotta MT, Wilson DB (1990) Oligomerization of the bacteriophage lambda S protein in the inner membrane of *Escherichia coli*. *J Bacteriol* 172:912–921.
36. Chang CY, Nam K, Young R (1995) *S* gene expression and the timing of lysis by bacteriophage lambda. *J Bacteriol* 177:3283–3294.
37. Smith DL, Struck DK, Scholtz JM, Young R (1998) Purification and biochemical characterization of the lambda holin. *J Bacteriol* 180:2531–2540.
38. Campbell A (1961) Sensitive mutants of bacteriophage lambda. *Virology* 14:22–32.
39. Goldberg AR, Howe M (1969) New mutations in the *S* cistron of bacteriophage lambda affecting host cell lysis. *Virology* 38:200–202.
40. Blattner FR, et al. (1997) The complete genome sequence of *Escherichia coli* K-12. *Science* 277:1453–1462.
41. Datsenko KA, Wanner BL (2000) One-step inactivation of chromosomal genes in *Escherichia coli* K-12 using PCR products. *Proc Natl Acad Sci USA* 97:6640–6645.
42. Saxton WO, Baumeister W, Hahn M (1984) Three-dimensional reconstruction of imperfect two-dimensional crystals. *Ultramicroscopy* 13:57–70.
43. Kremer JR, Mastronarde DN, McIntosh JR (1996) Computer visualization of three-dimensional image data using IMOD. *J Struct Biol* 116:71–76.
44. Frangakis AS, Hegerl R (2001) Noise reduction in electron tomographic reconstructions using nonlinear anisotropic diffusion. *J Struct Biol* 135:239–250.

MICROBIOLOGY